Journal of the Iranian Chemical Society (2022) 19:4589–4599
https://doi.org/10.1007/s13738-022-02623-7

ORIGINAL PAPER

Transparent and robust omniphobic surface using colloidal polymer layers

Tahereh Mahvelati-Shamsabadi[1] · Elaheh K. Goharshadi[1,2,3] · Gholamhossein Zohuri[1] · Reza Erfani Ghorbani[1] · Pedram Hosseinpour[1]

Received: 11 May 2022 / Accepted: 10 July 2022 / Published online: 26 July 2022

Abstract

Herein, the transparent omniphobic coating on glass slides was fabricated by using three different colloidal dispersions as sacrificial templates for a silica sol to make nano-scale surface roughness. These surface structures were further functionalized with a long chain fluorinated silane. These coatings showed a stable repellency to both water and low-surface tension liquids with the maximum contact angle of 156° to water and of about 130° to corn and paraffin oils. The prepared glass slides presented very high transparency with a light transmittance of about 92–98%. The coated surfaces were stable up to 400 °C and represented a good resistance under corrosive conditions by immersing 24 h in aqueous solutions of H_2SO_4 (pH 2) and KOH (pH 14).

Keywords Omniphobic surface · Water contact angle · Heptane repellency · Thermal stability

Introduction

The superhydrophobic surfaces can be fabricated if they have low surface energy and roughness on nano- and micro-scale [1–5]. However, the surfaces are wetted by organic liquids such as surfactant-based solutions, alcohols, or alkanes. The design of surfaces repellent to both high and low-surface tension liquids is of great importance since they have several applications including in self-cleaning, antiadhesion, stain-free, anti-fogging, seperation of oils and organic solvents from water, and anti-corrosion surfaces [6–10]. Omniphobic surfaces repel virtually everything including water, organic solvents, and oils [11–13]. They have several applications such as coatings for industrial equipment or in medical devices [14, 15]. Omniphobic surfaces can prevent the growth of bacteria and viruses [16–18]. The design of superhydrophobic surface has been inspired by nature especially lotus leaves [19, 20]. The most important principle in creating such surfaces is the reduction of contact points of liquid droplet with the surface [21, 22]. The roughness of a surface plays a critical role in obtaining Cassie–Baxter state [23]. In this state, the liquid droplet cannot touch the surface completely because of the presence of air bubbles trapped in surface roughness [24, 25]. After making surface roughness, the surface energy of surface should be reduced through functionalization by low surface energy materials [26].

Up to now, several omniphobic and superomniophobic surfaces with a very complex surface structure were designed [27–32]. Choi et al. [30] used localized photofluidization of azo polymers to fabricate doubly re-entrant nanostructures and superomniphobic surfaces. The azopolymer micropillars were reconfigured to a mushroom-like head with a doubly re-entrant nano-geometry by exposing to circularly polarized light. Wu et al. [33] designed a bioinspired of three-dimensional tribrachia-post-arrays with re-entrant geometry as a superhydrophobic and oleophobic polymer film or surface. Boban et al. [8] prepared substrate-independent, smooth, and omniphobic surface coating composed of fluorinated polyurethane and fluorodecyl polyhedral oligomeric silsesquioxane. Solvents with different surface tensions including water, hexadecane, ethanol, and silicone oil have low contact angle hysteresis (< 15°) on these surfaces,

✉ Elaheh K. Goharshadi
gohari@um.ac.ir

[1] Department of Chemistry, Faculty of Science, Ferdowsi University of Mashhad, Mashhad 9177948974, Iran

[2] Nano Research Center, Ferdowsi University of Mashhad, Mashhad 9177948974, Iran

[3] Micro-Nano Technologies in Renewable Energies Center, Ferdowsi University of Mashhad, Mashhad 9177948974, Iran

allowing liquid droplets to slide off and leaving no residue [34]. These robust surfaces retain their repellent properties more effectively than textured or lubricated omniphobic surfaces exposed to mechanical abrasion [8]. Zhue et al. [35] designed the omniphobic surfaces combining excellent liquid repellency and remarkable durability using a bottom-up microfluidic emulsion templating technique. They interconnected the resulting porous membranes with solid structures and uniform honeycomb-like micro-cavities containing narrow openings. The solid/liquid contact area was precisely controlled through the membrane pore size. The resulting omniphobic surfaces were mechanically and chemically durable. Tuteja et al. [36] fabricated the surfaces with reentrant texture to support strongly the metastable composite solid–liquid–air interfaces. The prepared surfaces could support a robust composite interface with essentially every liquid. The making of the surfaces with this topography is very complex and expensive.

Transparency is another vital feature of an omniphobic surface [37, 38]. However, the preparation of transparent omniphobic films is not easy because the transparency decreases due to the Mie effect, i.e. the elastically scattered light by particles with a diameter equal or greater than the incident light wavelength [39]. Such limitation makes the fabrication of omniphobic and transparent films on glass substrates difficult. Hence, the surface roughness should be accurately controlled. The surface roughness should be large enough to show the omniphobicity and as low as to maintain transparency [40]. Also, the surface roughness should be in the nano-scale comparable to the wavelength of the visible light [41].

Herein, we aim to design a simple and economy fractal structure with an omniphobic property on glass slides using a colloidal deposition. In our approach, a colloidal layer is masked on glass slides by a silica sol to form an inverse replica. Then, the surface is functionalized by a fluoroalkyl trichlorosilane. The dangling bonds of the fluoroalkyl chain interact with other chemicals through van der Waals interactions.

Materials and methods

Materials

Styrene (99.9%, Merck), methyl methacrylate (MMA, 99%, Merck), butyl acrylate (BA, 98%, Merck), vinyl acetate (VA, 99%, Merck), ammonium persulfate (APS, 98%, Merck), sodium dodecyl sulfate (SDS, 99%, Merck), hydrochloric acid (37%, Merck), ethanol (98%, Merck), acetone (97%, KUMHO P&B, Korea), isopropanol (70%, Mojallali), sulfuric acid (95–98%, Merck), hydrogen peroxide (30%, Merck), tetraethylorthosilicate (TEOS) (98%,, Sigma-Aldrich), 1H,1H,2H,2H-Perfluorododecyl-trichlorosilane (97%, Sigma-Aldrich), and commercial Kenon 30 were used as received. The standard microscopy glass slides were used as a glass substrate. The deionized water (DI) was used for the preparation of all solutions.

Colloidal synthesis

Three different colloidal dispersions were prepared by emulsion and soap-free emulsion polymerization (Table 1). The similar procedure was used for all dispersions. Of course, the surfactants were not used for vinyl acetate (VA) colloidal dispersion. DI water was heated to 70 °C. The monomers, initiator, and the surfactants were divided into two parts (A and B). Then, the water was added to each of these two parts in two beakers and vigorously stirred for 10 min. After that, part A was added to the reactor and stirred for 30 min at 70 °C. Part B was injected to the reaction medium through a dropping funnel in 2.5 h. The polymerization was carried out for 3 h at 70 °C. The temperature was controlled through the reaction sliding angle measurements. After cooling to room temperature, the dispersion was stored in a refrigerator until its use.

Cleaning the glass slides

The glass slides were cleaned by liquid soap, ethanol, acetone, isopropanol, and DI water in sequence in an ultrasonic bath 10 min for each solvent. After that, they were immersed in acid piranha solution (1:3 (v/v) of H_2O_2 and H_2SO_4), followed by heating until no bubbles were released and then rinsed with DI. Then, the clean glass slides were put under UV lamp (400 W) for 1 h.

Table 1 Different synthetic polymers and their preparation methods

Colloidal type	Monomers	Initiator	Surfactants	Synthesis method
VA		APS	–	Soap-free emulsion
S-BA	Styrene, butyl acrylate	APS	SDS, Kenon 30	Emulsion
S-MMA	Styrene, methyl meta acrylate	APS	SDS, Kenon 30	Emulsion

Formation of colloidal layers on glass slides

The colloidal layers were crystallized by spin coating. 100 µL of 5% wt ethanolic colloidal solution was spin coated on the glass slide at 300, 600, and 2000 rpm for 12, 2, and 12 s in sequence. Then, the glass slides dried under an angle of approximately 45°. All prepared colloidal films were dried at 60 °C in an electrical oven for 2 h.

Deposition of silica sol on colloidal layer

A solution of TEOS, HCl (0.1 M), and ethanol with weight ratios of 1:1:1.5 was prepared and refluxed for 1 h at 70 °C. Then, the TEOS solution was diluted with ethanol (Table 2). After that, 50 µL of diluted solution was spin coated onto the colloidal covered substrate (2.5×2.5 cm^2) at 3000 rpm for 30 s. The colloidal layers were removed by combustion at 500 °C by ramping from room temperature to 500 °C for 5 h and then 2 h at 500 °C.

Fluorosilanization

Prior to silanization, the substrates were cleaned in an acid piranha. Then, fluorosilanization was carried out by immersion of glass slides in the solution of 0.01 mM of 1H,1H,2H,2H-perfluorododecyl-trichlorosilane in hexane for 3 h at room temperature. Then, the glass slides were withdrawn and heated to 70 °C.

Test for corrosive resistance

For the long-term application of coated surfaces, their resistance ability against corrosive liquids is important. For this purpose, the coated glass slide was immersed in an aqueous H_2SO_4 (pH = 2.0) and KOH (pH = 14.0) solution for several hours.

Instruments

An ultrasonic bath (40 kHz) was used for samples preparation. The prepared glass slides were dried with vacuum drying oven model (VS 1202V5). The spin coater [Modern Technology Development Institute model (2 M.T.D.1.92)] was used for colloidal and silica deposition on glass substrate. For contact angle measurements, a water droplet (10 µL) was dropped with a sampler carefully onto the glass surface.The field emission scanning electron microscopy (FE-SEM) analysis of the samples was taken by MIRA3 TESCAN (Boo-Ali Institute, Mashhad, Iran). The atomic force microscopy (AFM) images of the samples deposited on a mica substrate were obtained by Ara Research (model no. 0101/A, Iran) in a non-contact mode at room temperature. The transmittance spectra were recorded using a Unico UV-2100 spectrophotometer. The spectra were recorded in air within the range of 400–1000 nm. Images were captured with a camera (Canon SX200, Japan) and then analyzed using Image J software for acquiring contact angle. The sliding angle measurements were conducted with a simple designed device which had a movable plane for tilting glass substrate until water droplet (10 µL) start to roll off.

Table 2 The ratios of TEOS and ethanol used for spin-coating of silica sol-gel solution

Colloidal type	TEOS: Ethanol volume ratio
VA	1:9
S-BA	1:15
S-MMA	1:20

Results and discussion

Characterization

Figure 1a–c shows the particle size distribution (PSD) of three different of as-prepared colloidal dispersions. As these figures depicted, the average size of prepared colloidal particles was estimated to be about 30, 100, and 300 nm for styrene-methyl methacrylate (S-MMA), S-BA (styrene-butyl acrylate), and vinyl acetate (VA), respectively. There is an obvious polydispersity in these colloids.

Figure 2a–c shows the FE-SEM images of prepared colloidal layer structures on glass slides. These figures show different polymers produce unlike patterns on the glass slide. Using these three colloidal layers as the templates, we constructed three different roughness structures on glass surface. After burning the polymer templates, a fractal-like structure was appeared as it is illustrated in Fig. 2d–f. These images show that the porous layer has a roughness in the range of nanoscales.

To gain a better insight on surface morphology, the AFM images were also taken (Fig. 3a–c). The 2D and 3D AFM images show that the surfaces of substrates were coated homogeneously by silica nanoparticles (NPs) in the range of nanometer. The images also confirm the production of three different patterns using different colloidal dispersions. Silica NPs are decorated on a glass surface based on the patterns dictated by colloidal dispersion.

The roughness parameters of *Ra* (average surface roughness) and *Rq* (root mean square of roughness) of the prepared surfaces were calculated using AFM data and shown in Table 3. Table 3 confirms a very thin rough layer of silica NPs in the range of nanometer was produced on a glass surface.

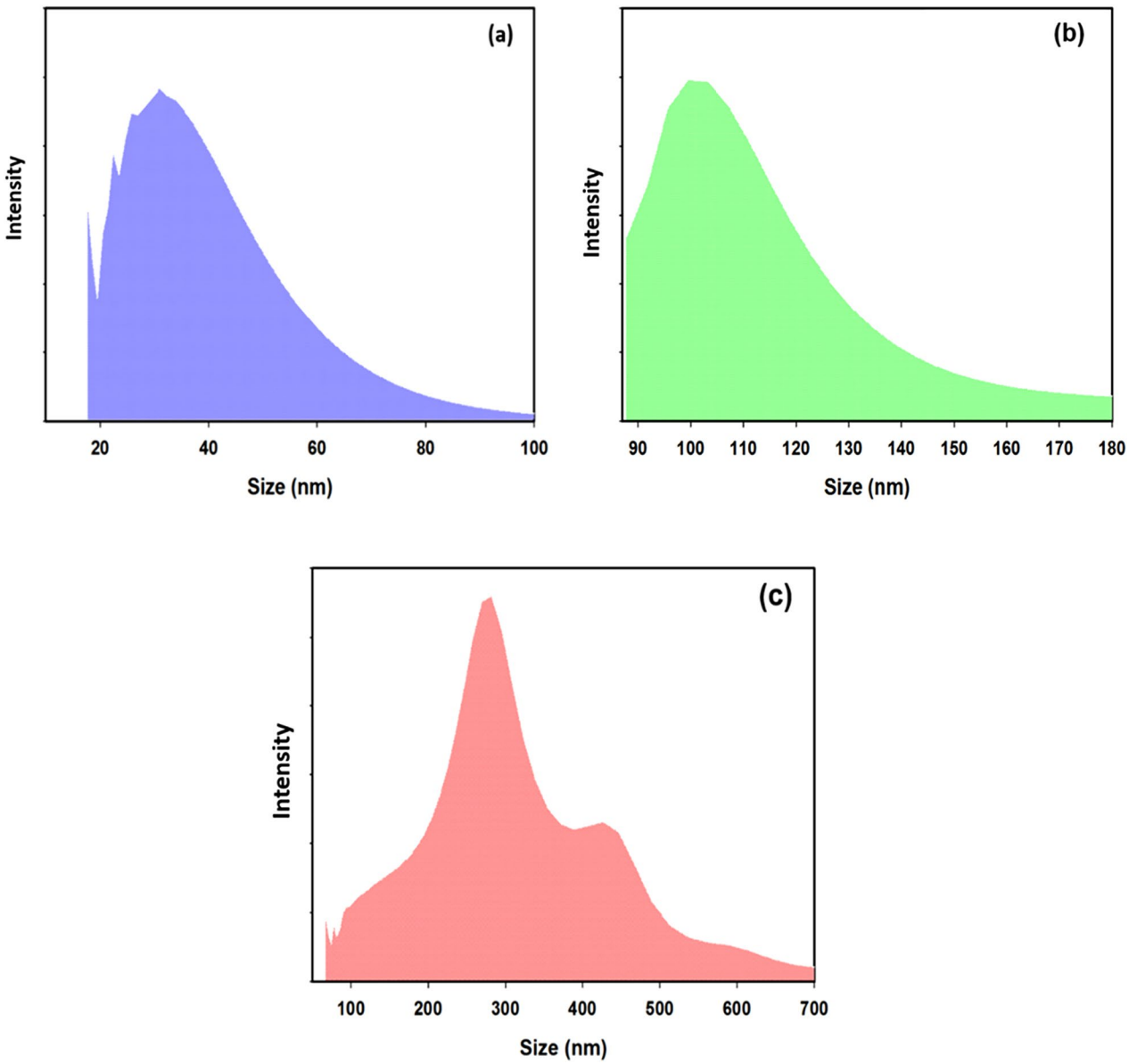

Fig. 1 PSD of three colloidal particles **a** S-MMA, **b** S-BA and **c** VA

Figure 4a–c show the transmission spectra of the VA, S-BA, and S-MMA on glass slides prepared through spin-coating. The glass slide with VA geometry showed a little coloration under the light due to Mie effect. Mie scattering occurs only the size of the scattering particles is comparable to the wavelength of the light rather than much smaller or much larger in the fractal structure [6, 42]. As Fig. 4a shows the transmittance of VA glass slide is less than plain glass slide for all wavelengths due to the increase in light reflections. Meanwhile, light reflection strongly reduced for S-BA and S-MMA (Fig. 4b and c) and the glass slide transparency is identical. For S-BA structure, the reflection of incident light vanishes and the light is transmitted completely through the glass. In other words, the difference between the air refractive index and the coated glass decreases. Hence, the glass slide can show an anti-refractive property. Compared to the bare glass slide, the S-BA structure can suppress the reflectance obviously due to the low refractive index. This is due to the new interference formation between the light reflected from the different interfaces of air–particle and particle–substrate. However, the rough structure including micro and NPs greatly decreased the reflection with respect to the bare glass. This is as a result of multiple reflections which occur between the different interfaces of air–NPs, NPs–micro-particles, and micro-particles–substrate. Hence, the longer light traveling distances reduce the energy loss

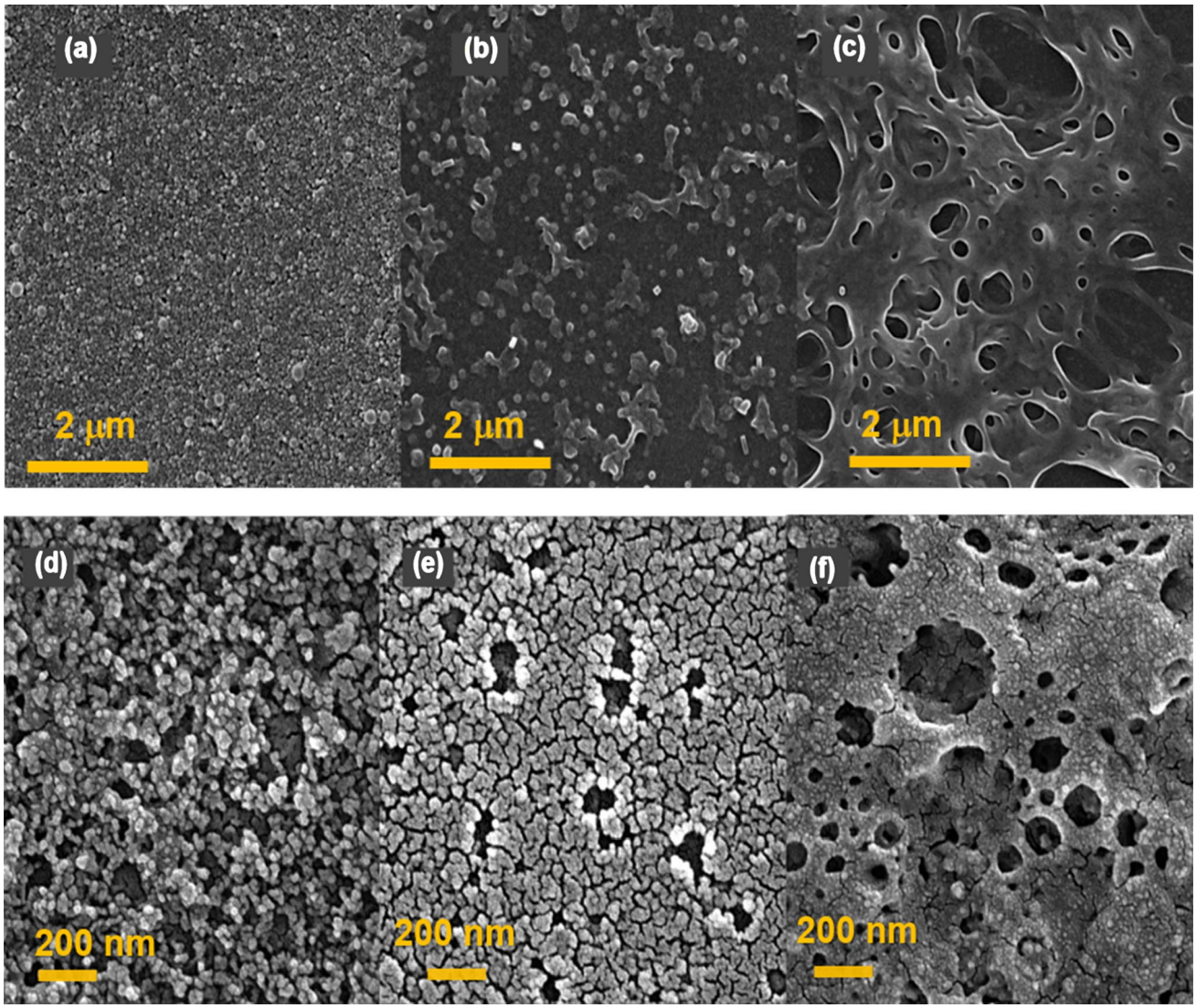

Fig. 2 FE-SEM images of three different colloidal templates of **a** S-MMA, **b** S-BA and **c** VA before combustion. The roughness structure of **d** S-MMA, **e** S-BA and **f** VA after combustion

and decrease reflection. The transparency of S-MMA coated glass slide is better than that of VA, but its transparency is a little less than that of plain glass. The best transparency and the lowest reflection are due to S-BA structure because of its more uniform surface compared to the S-MMA with more agglomeration of SiO_2 particles. For VA, the porosity size for the structure is much greater than 100 nm. Hence, the reflection increases and the anti-refractive property reduced due to Mie effect.

Wetting property

The wetting property of the prepared glass substrate was tested by measuring the static contact angle and the minimum sliding angle for some liquids under different conditions.

Effect of different roughness topography

The static contact angle and the minimum sliding angle for 10 µL of four liquids including water, paraffin oil, edible oil, and heptane on three structures of VA, S-BA, and S-MMA are shown in Fig. 5a and b, respectively, See also Video S1 for heptane. As these figures show, there is no an obvious difference between the static contact angle and the sliding angle in these structures. It means that all structures follow the Cassi–Baxter state because the air pockets in the roughness of the surface prevent the infiltration of the liquid droplet into the rough structure. Subsequently,

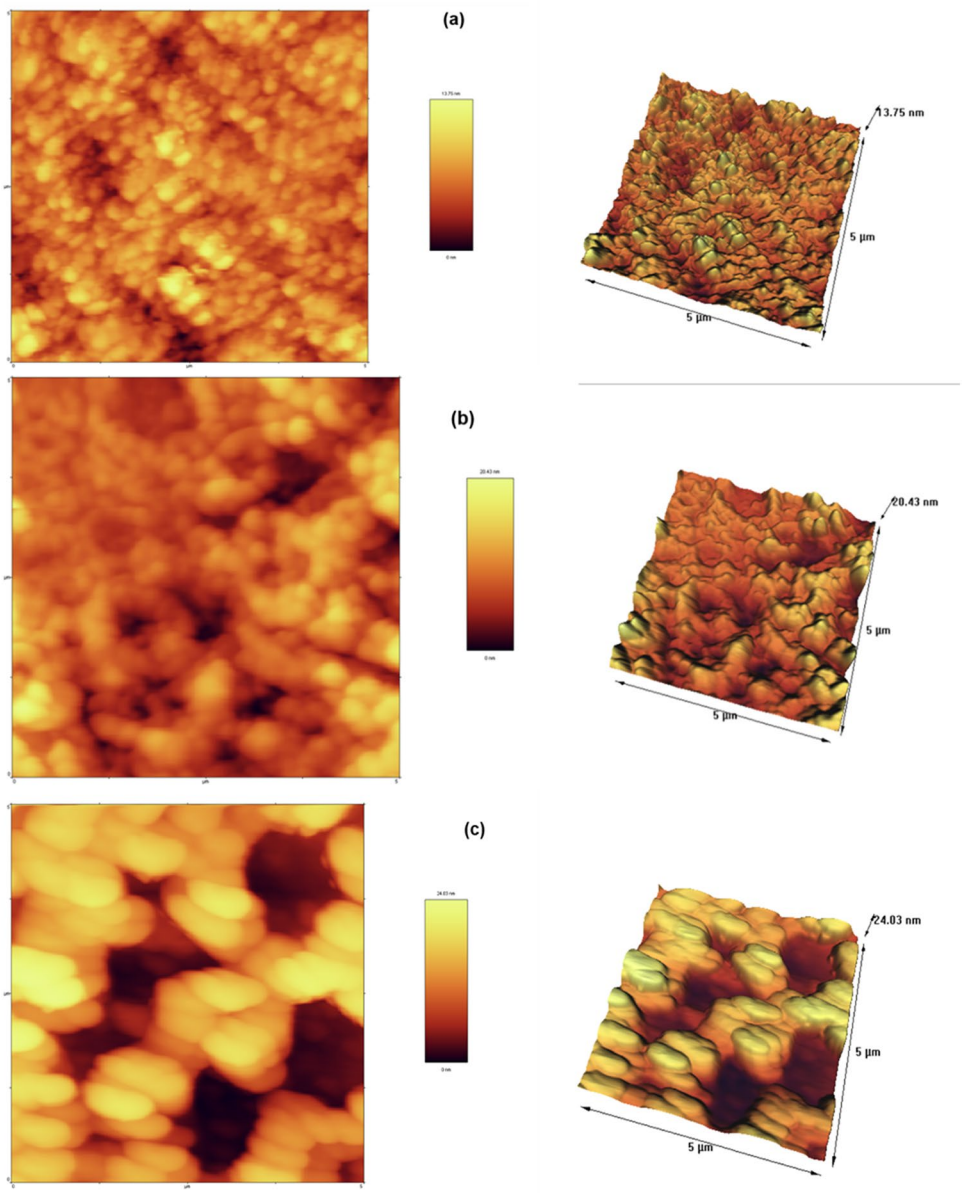

Fig. 3 The AFM images of **a** S-MMA, **b** S-BA, and **c** VA after colloid combustion on the glass slide

Table 3 Roughness parameters

Surface structure	*Ra* (nm)	*Rq* (nm)	Thickness (nm)
VA	4.97	5.87	24.03
S-BA	3.93	4.72	20.43
S-MMA	2.30	2.95	13.75

the liquid droplet forms a very high contact angle and does not pin to the surface. While in Wenzel state, the liquid penetrates the rough structure. Hence, the contact angle decreases for liquid [25].

For the next experiments, the glass slide with S-BA structure was chosen due to its high transparency and anti-reflective property.

Effect of liquid surface tension

The influence of the liquid surface tension on the wetting property of S-BA surface was evaluated by measuring the static contact angle and the minimum sliding angle of organic solvents with different surface tensions (Fig. 6a and b). After fluorosilanization and heating at 70 °C, the static contact angle of 156° was formed with the sliding angle less than 1°. It was very difficult to deposit water droplets on the surface because they were immediately rolled off. The

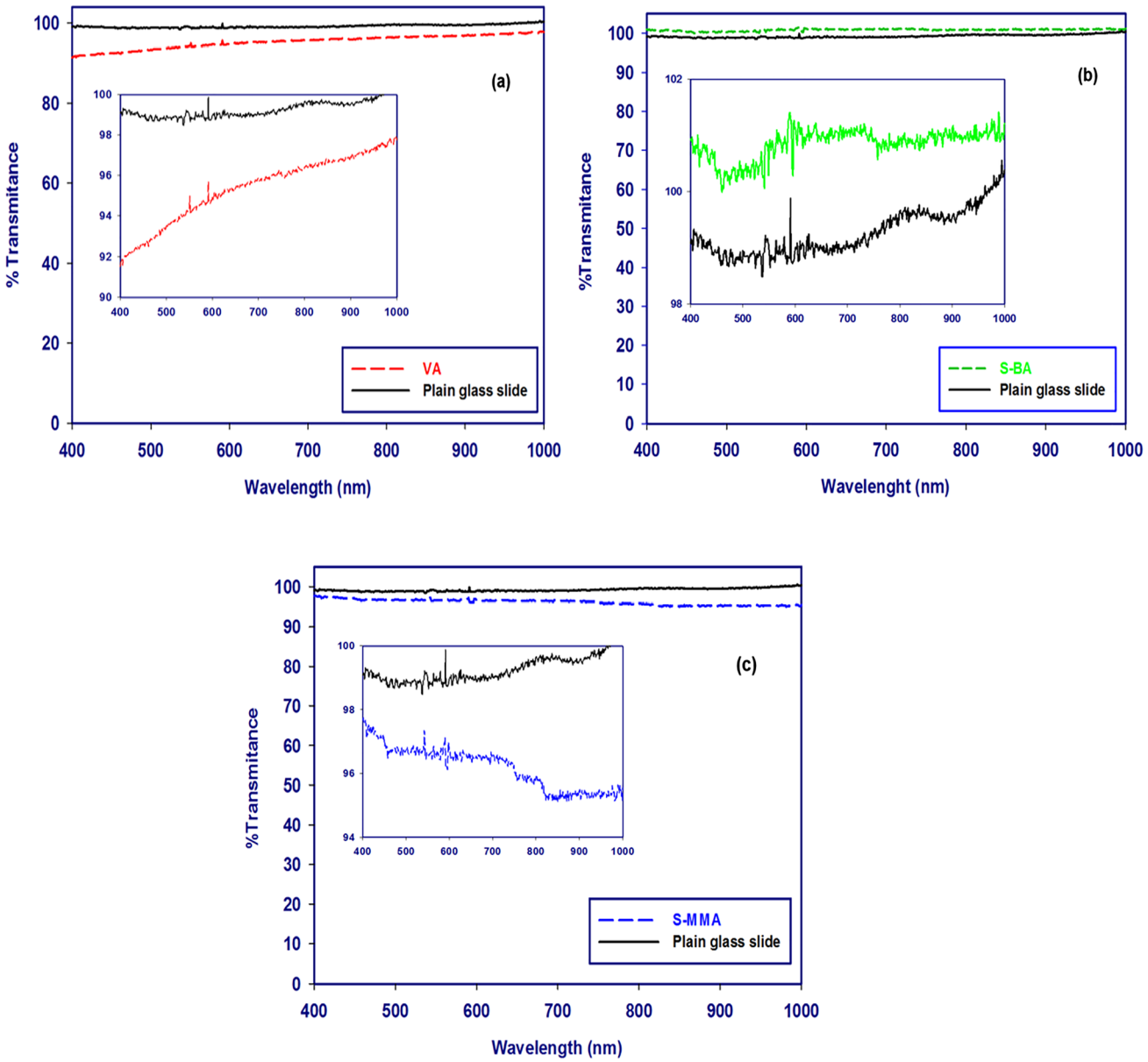

Fig. 4 The optical property of microscopic slides covered with three different roughness structures **a** VA, **b** S-BA, **c** S-MMA

sliding angle increased up to 10° after washing. This is due to the presence of un-bonded fluoroalkyl silane layers on the surface which destroyed after washing. These layers have a very loose bond with the surface. For organic solvents, the maximum contact angle was about ~ 134° for paraffin and edible oil with the surface tension of 48 and 32 mN/m, respectively. For heptane (20.14 mN/m), the contact angle dramatically decreased to about 50° (Fig. 6a). A droplet of ethanol completely spread on the glass surface and wet the surface. Also, we checked ethanol with the surface tension of (22 mN/m). The values of the contact angles for water, two oils (paraffin and edible oils), and heptane suggest that S-BA surface follows Cassie–Baxter wetting state. For ethanol, a Wenzel wetting state was formed and it completely touched the surface. It means infiltration of the ethanol into the microscopic pores occurs. By liquid-infiltration into the porous structure of the surface, the contact angle reduces to a lower amount because of the transition from Cassie–Baxter to Wenzel wetting [16]. The minimum sliding angle is about 10° for water and increases to 15° for two oils. Although the heptane contact angle was low, it did not wet the glass surface. It slided off on a glass with a sliding angle of about 11°–15° (Video S1).

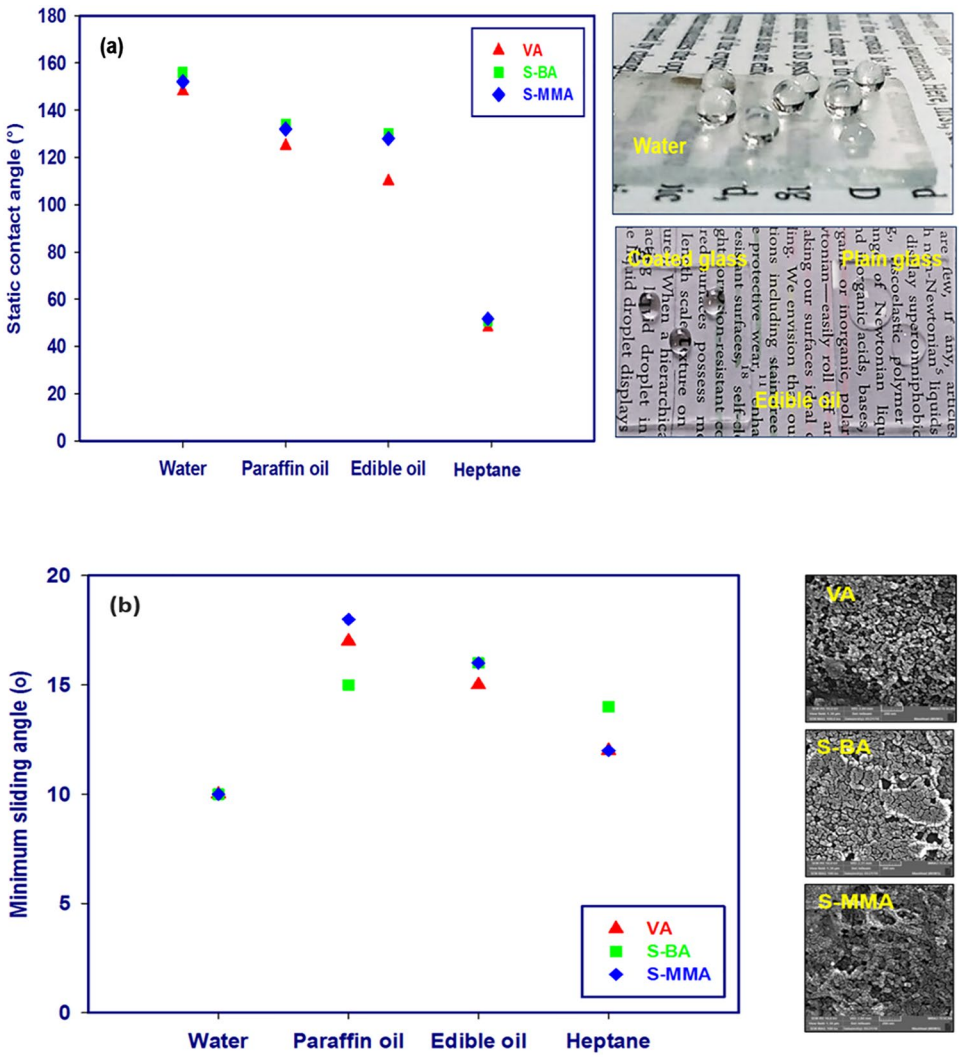

Fig. 5 **a** The static water contact angle **b** the minimum sliding angle for a droplet of 10 µL of four liquids including water, paraffin oil, edible oil, and heptane on three structures of VA, S-BA, and S-MMA

Stability measurements

Effect of thermal treatment and long-term storage

To investigate the thermal resistance of surface, the coated glass slides were sintered at 100, 300, 500, and 700 °C, ramped at 2 °C min^{-1} from room temperature to specified temperature for 2 h and then ramped down to room temperature. Then, the wetting property of the samples was measured. As shown in Fig. 7a, the water contact angle did not change up to 300 °C for water and oil. When temperature increased from 300 to 700 °C, the water contact angle gradually decreased. The fluorosilane layer was decomposed by annealing at temperatures greater than 300 °C. The annealed coatings again recovered their omphiphobicity by fluorosilanization. This confirms the stability of the rough structure due to strong covalent bonds between silica structure of the prepared coating and glass surface. Heating at high temperatures cannot destroy the silica coating layer because Si–O–Si bonds are very strong. These bonds are broken at temperatures greater than 300 °C. Meanwhile, the organic layer is much weaker and did not destroy at lower temperatures.

The long-term stability of heptane repellency on horizontally stored substrates is investigated and shown in Fig. 7b. The sliding angle was measured of about 10°–15° even after 6 months.

Effect of corrosive condition

Figure 8 shows the contact angle for water and paraffin oil after immersing the S-BA glass slide in H_2SO_4 (1 M) and KOH (1 M) solutions did not change after 24 h. After this time, it started to decrease gradually. The coated glass slide is omphiphobic and is covered with a layer of air pad. The air layer can prevent the glass slide from wetting by corrosive H_2SO_4 and KOH solutions. However, the air layer gradually disappeared with increase in immersion time as

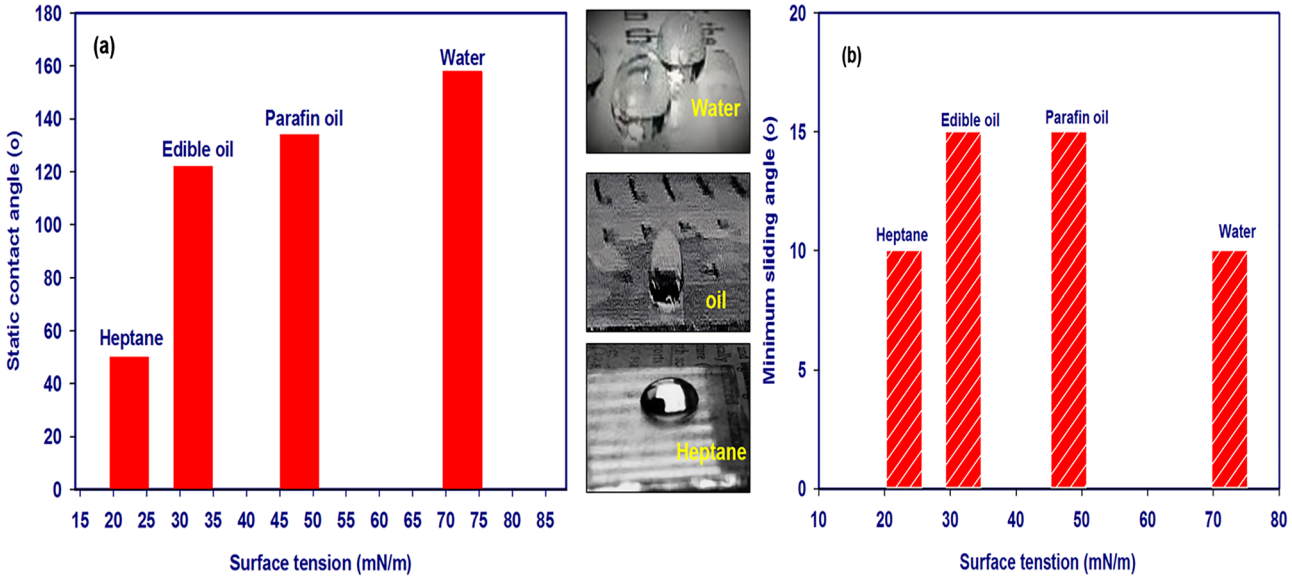

Fig. 6 The effect of different liquids with different surface tensions on **a** static contact angle and **b** minimum sliding angle

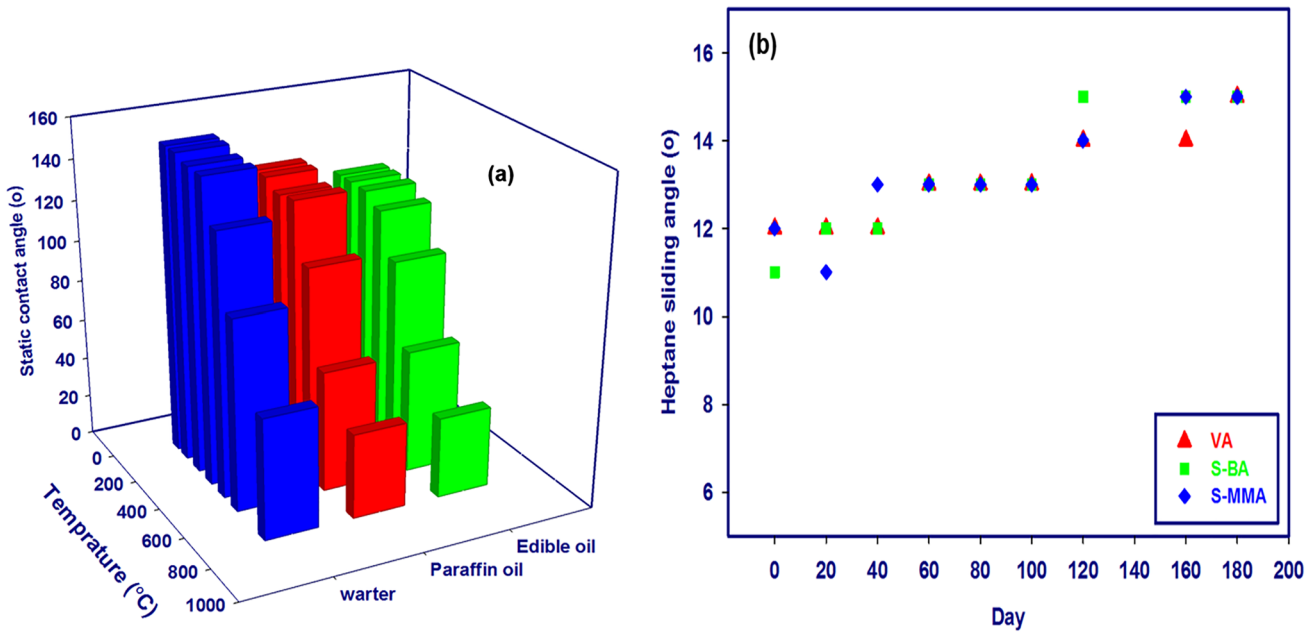

Fig. 7 **a** The static water contact angle versus temperature of three different liquids with different surface tensions for coated glass slide (S-BA), **b** the heptane sliding angle versus day of storage of three different colloidal types VA, S-BA, and S-MMA

a result of the fluid-air exchange. It caused the glass slides were wetted.

Conclusion

Three different types of colloidal polymer templates were prepared as sacrificial patterns for creating roughness on

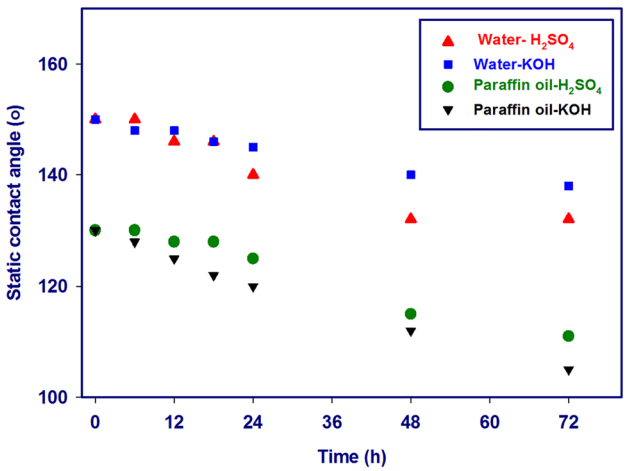

Fig. 8 Static contact angle measurements of water and paraffin oil on the S-BA glass slide after immersion in H_2SO_4 (1 M) and KOH (1 M) solutions

glass slide. A silica sol was masked on these soft templates. Silica NPs were decorated on the glass surface based on the patterns dictated by colloidal dispersions. After fluorosilanization the glass slides, they presented good repellency to both water and low-surface tension organic solvents. The prepared omniphobic glass slides had high transparency for visible light and showed good thermal stability up to 300 °C. The samples showed good stability under corrosive conditions. Hence, these robust and highly transparent omniphobic surfaces can be good candidates for a variety of applications such as self-cleaning, anti-icing, antifogging, and stain-free surfaces.

Supplementary Information The online version contains supplementary material available at https://doi.org/10.1007/s13738-022-02623-7.

Acknowledgements The authors express their gratitude to the Ferdowsi University of Mashhad for support of this project (Grant No. 3/38438).

References

1. L. Xu, J. He, Fabrication of highly transparent superhydrophobic coatings from hollow silica nanoparticles. Langmuir **28**, 7512–7518 (2012)
2. T. Rezayi, M.H. Entezari, Achieving to a superhydrophobic glass with high transparency by a simple sol–gel-dip-coating method. Surf. Coat. Technol. **276**, 557–564 (2015)
3. T. Rezayi, M.H. Entezari, Wettability properties vary with different morphologies of ZnO nanoparticles deposited on glass and modified by stearic acid. New J. Chem. **40**, 2582–2591 (2016)
4. D. Wang, Q. Sun, M.J. Hokkanen, C. Zhang, F.-Y. Lin, Q. Liu, S.-P. Zhu, T. Zhou, Q. Chang, B. He, Design of robust superhydrophobic surfaces. Nature **582**, 55–59 (2020)
5. F. Chen, J. Du, S. Huang, Fabrication of repairable anti-corrosive superhydrophobic surfaces with micro-nano structures by ultrasonic cavitation. Appl. Surf. Sci. **541**, 148605 (2021)
6. N. Vogel, R.A. Belisle, B. Hatton, T.-S. Wong, J. Aizenberg, Transparency and damage tolerance of patternable omniphobic lubricated surfaces based on inverse colloidal monolayers. Nat. Commun. **4**, 1–10 (2013)
7. Y. Si, Z. Guo, Superhydrophobic nanocoatings: from materials to fabrications and to applications. Nanoscale **7**, 5922–5946 (2015)
8. M. Boban, K. Golovin, B. Tobelmann, O. Gupte, J.M. Mabry, A. Tuteja, Smooth, all-solid, low-hysteresis, omniphobic surfaces with enhanced mechanical durability. ACS Appl. Mater. Interfaces. **10**, 11406–11413 (2018)
9. A. Jamsaz, E. K. Goharshadi, A. Barras, M. Ifires, S. Szunerits, R. Boukherroub, Magnetically driven superhydrophobic/superoleophilic graphene-based polyurethane sponge for highly efficient oil/water separation and demulsification. Sep. Purif. Technol. **274**, 118931 (2021)
10. P. Mandal, J. Ivvala, H.S. Arora, S.K. Ghosh, H.S. Grewal, Bioinspired micro/nano structured aluminum with multifaceted applications. Colloids Surf. B Biointerfaces. **211**, 112311 (2022)
11. T.-S. Wong, S.H. Kang, S.K.Y. Tang, E.J. Smythe, B.D. Hatton, A. Grinthal, J. Aizenberg, Bioinspired self-repairing slippery surfaces with pressure-stable omniphobicity. Nature **477**, 443–447 (2011)
12. R. Hensel, C. Neinhuis, C. Werner, The springtail cuticle as a blueprint for omniphobic surfaces. Chem. Soc. Rev. **45**, 323–341 (2016)
13. E. Arzt, H. Quan, R.M. McMeeking, R. Hensel, Functional surface microstructures inspired by nature—from adhesion and wetting principles to sustainable new devices. Prog. Mater. Sci. **120**, 100823 (2021)
14. D.C. Leslie, A. Waterhouse, J.B. Berthet, T.M. Valentin, A.L. Watters, A. Jain, P. Kim, B.D. Hatton, A. Nedder, K. Donovan, A bioinspired omniphobic surface coating on medical devices prevents thrombosis and biofouling. Nat. Biotechnol. **32**, 1134–1140 (2014)
15. M. Villegas, Y. Zhang, N. Abu Jarad, L. Soleymani, T.F. Didar, Liquid-infused surfaces: a review of theory, design, and applications. ACS Nano **13**, 8517–8536 (2019)
16. A.K. Kota, G. Kwon, A. Tuteja, The design and applications of superomniphobic surfaces. NPG Asia Mater. **6**, e109–e109 (2014)
17. Y. Lu, G. He, C.J. Carmalt, I.P. Parkin, Synthesis and characterization of omniphobic surfaces with thermal, mechanical and chemical stability. RSC Adv. **6**, 106491–106499 (2016)
18. S.M. Imani, L. Ladouceur, T. Marshall, R. Maclachlan, L. Soleymani, T.F. Didar, Antimicrobial nanomaterials and coatings: current mechanisms and future perspectives to control the spread of viruses including SARS-CoV-2. ACS Nano **14**, 12341–12369 (2020)
19. D. Zhang, L. Li, Y. Wu, B. Zhu, H. Song, One-step method for fabrication of bioinspired hierarchical superhydrophobic surface with robust stability. Appl. Surf. Sci. **473**, 493–499 (2019)
20. Z. Altangerel, B. Purev-Ochir, A. Ganzorig, T. Tsagaantsooj, G. Lkhamsuren, A. Choisuren, G. Chimed, Superhydrophobic modification and characterization of cashmere fiber surfaces by wet coating techniques of silica nanoparticles. Surf. Interfaces. **19**, 100533 (2020)
21. A. Tuteja, W. Choi, M. Ma, J.M. Mabry, S.A. Mazzella, G.C. Rutledge, G.H. McKinley, R.E. Cohen, Designing superoleophobic surfaces. Science (80-.) **318**, 1618–1622 (2007)
22. Y. Zhang, B. Dong, S. Wang, L. Zhao, L. Wan, E. Wang, Mechanically robust, thermally stable, highly transparent superhydrophobic coating with low-temperature sol–gel process. RSC Adv. **7**, 47357–47365 (2017)
23. X. Zhang, B. Ding, Y. Bian, D. Jiang, I.P. Parkin, Synthesis of superhydrophobic surfaces with Wenzel and Cassie-Baxter state: experimental evidence and theoretical insight. Nanotechnology **29**, 485601 (2018)

24. D. Goswami, S.K. Medda, G. De, Superhydrophobic films on glass surface derived from trimethylsilanized silica gel nanoparticles. ACS Appl. Mater. Interfaces. **3**, 3440–3447 (2011)
25. X. Deng, L. Mammen, H.-J. Butt, D. Vollmer, Candle soot as a template for a transparent robust superamphiphobic coating. Science (80-.) **335**, 67–70 (2012)
26. I. Jerman, M. Koželj, B. Orel, The effect of polyhedral oligomeric silsesquioxane dispersant and low surface energy additives on spectrally selective paint coatings with self-cleaning properties. Sol. Energy Mater. Sol. Cells. **94**, 232–245 (2010)
27. P. Kim, T.-S. Wong, J. Alvarenga, M.J. Kreder, W.E. Adorno-Martinez, J. Aizenberg, Liquid-infused nanostructured surfaces with extreme anti-ice and anti-frost performance. ACS Nano **6**, 6569–6577 (2012)
28. H.-J. Choi, S. Choo, J.-H. Shin, K.-I. Kim, H. Lee, Fabrication of superhydrophobic and oleophobic surfaces with overhang structure by reverse nanoimprint lithography. J. Phys. Chem. C. **117**, 24354–24359 (2013)
29. S. Utech, K. Bley, J. Aizenberg, N. Vogel, Tailoring re-entrant geometry in inverse colloidal monolayers to control surface wettability. J. Mater. Chem. A. **4**, 6853–6859 (2016)
30. J. Choi, W. Jo, S.Y. Lee, Y.S. Jung, S.-H. Kim, H.-T. Kim, Flexible and robust superomniphobic surfaces created by localized photofluidization of azopolymer pillars. ACS Nano **11**, 7821–7828 (2017)
31. Z. Zhang, H. Wang, Y. Liang, X. Li, L. Ren, Z. Cui, C. Luo, One-step fabrication of robust superhydrophobic and superoleophilic surfaces with self-cleaning and oil/water separation function. Sci. Rep. **8**, 1–12 (2018)
32. J.A. Kharraz, M.U. Farid, N.K. Khanzada, B.J. Deka, H.A. Arafat, A.K. An, Macro-corrugated and nano-patterned hierarchically structured superomniphobic membrane for treatment of low surface tension oily wastewater by membrane distillation. Water Res. **174**, 115600 (2020)
33. Y. Wu, S. Zhou, B. You, L. Wu, Bioinspired design of three-dimensional ordered tribrachia-post arrays with re-entrant geometry for omniphobic and slippery surfaces. ACS Nano **11**, 8265–8272 (2017)
34. J. Liu, Y. Sun, X. Zhou, X. Li, M. Kappl, W. Steffen, H. Butt, One-step synthesis of a durable and liquid-repellent poly (dimethylsiloxane) coating. Adv. Mater. **33**, 2100237 (2021)
35. P. Zhu, T. Kong, X. Tang, L. Wang, Well-defined porous membranes for robust omniphobic surfaces via microfluidic emulsion templating. Nat. Commun. **8**, 1–10 (2017)
36. A. Tuteja, W. Choi, J.M. Mabry, G.H. McKinley, R.E. Cohen, Robust omniphobic surfaces. Proc. Natl. Acad. Sci. **105**, 18200–18205 (2008)
37. Y. Sun, Z. Guo, Recent advances of bioinspired functional materials with specific wettability: from nature and beyond nature. Nanoscale Horizons. **4**, 52–76 (2019)
38. T.A.S. Mahmut, H. Memon, F. Xu, I. Ahmed, X. Hou, Electrospun nanofibre membrane based transparent slippery liquid-infused porous surfaces with icephobic properties. Colloids Surf. A Physicochem. Eng. Asp. **585**, 124177 (2020)
39. P. Tian, Z. Guo, Bioinspired silica-based superhydrophobic materials. Appl. Surf. Sci. **426**, 1–18 (2017)
40. S. Yu, Z. Guo, W. Liu, Biomimetic transparent and superhydrophobic coatings: from nature and beyond nature. Chem. Commun. **51**, 1775–1794 (2015)
41. N. Wang, D. Xiong, Comparison of micro-/nano-hierarchical and nano-scale roughness of silica membranes in terms of wetting behavior and transparency. Colloids Surf. A Physicochem. Eng. Asp. **446**, 8–14 (2014)
42. K.R. Phillips, G.T. England, S. Sunny, E. Shirman, T. Shirman, N. Vogel, J. Aizenberg, A colloidoscope of colloid-based porous materials and their uses. Chem. Soc. Rev. **45**, 281–322 (2016)